Coupling approach for the realization of a $\mathcal{PT}$-symmetric potential for a Bose-Einstein condensate in a double well

Fabian Single, Holger Cartarius,* Günter Wunner, and Jörg Main
Institut für Theoretische Physik 1, Universität Stuttgart, 70550 Stuttgart, Germany
(Received 26 September 2014; published 30 October 2014)

We show how non-Hermitian potentials used to describe probability gain and loss in effective theories of open quantum systems can be achieved by a coupling of the system to an environment. We do this by coupling a Bose-Einstein condensate (BEC) trapped in an attractive double-δ potential to a condensate fraction outside the double well. We investigate which requirements have to be imposed on possible environments with a linear coupling to the system. This information is used to determine an environment required for stationary states of the BEC. To investigate the stability of the system we use fully numerical simulations of the dynamics. It turns out that the approach is viable and possible setups for the realization of a $\mathcal{PT}$-symmetric potential for a BEC are accessible. Vulnerabilities of the whole system to small perturbations can be attributed to the singular character of the simplified δ-shaped potential used in our model.

DOI: 10.1103/PhysRevA.90.042123 PACS number(s): 11.30.Er, 03.75.Kk, 03.65.Ge

I. INTRODUCTION

In quantum mechanics the Hamiltonian is used to describe a system. It determines the energy levels of all eigenstates and defines the time evolution of a quantum state. It is common to work with Hermitian Hamiltonians to ensure that the energies are real valued and the total probability is preserved in time. These properties are no longer given for non-Hermitian Hamiltonians. They appear in effective theories of open quantum systems [1] and may have imaginary potentials that represent probability sources or drains.

A way to obtain real eigenvalues in non-Hermitian systems is to balance the total gain and loss. The simplest way to achieve this is by working with $\mathcal{PT}$-symmetric systems, i.e., systems in which the $\mathcal{PT}$ operator (consecutive execution of the time and parity operators) commutes with the Hamiltonian H. For a standard Hamiltonian of the form $H = p^2 + V(x)$ this is equivalent to the condition

$$V(x) = V^*(-x). \tag{1}$$

Great interest in non-Hermitian $\mathcal{PT}$-symmetric systems was generated by Bender and Boettcher in 1998 [2]. Since then, $\mathcal{PT}$-symmetric systems have been the subject of theoretical studies of quantum systems [3–6], quantum field theories [2,7–10], microwave cavities [11], electronic devices [12,13], and optical [14,15] systems. The stationary Schrödinger equation was solved for scattering solutions [4] and bound states [5]. Spectral singularities in $\mathcal{PT}$-symmetric potentials [16] turned out to be connected with the amplification of waves [17] and the lasing threshold [18]. Nonlinear $\mathcal{PT}$-symmetric quantum systems have been discussed for BECs described in a two-mode approximation [19–21] and in model potentials [22]. The first experimental realization was achieved in 2009–2010, when two groups observed the expected properties in optical systems [23,24]. While these optical systems are analogs of quantum mechanical systems, a real non-Hermitian *quantum* system has yet to be realized. A good candidate for such a realization is a BEC in a two-well potential as suggested by Klaiman *et al.* [25]. This potential is extended with asymmetric imaginary parts, representing a particle drain in one well and a particle source in the other. Theoretical investigations revealed that this $\mathcal{PT}$-symmetric system has observable eigenstates [19–21,26–31]. However, an experimental confirmation of these results cannot be made as long as there is no way to realize a non-Hermitian potential.

We approach this issue with a simple model. To render it most instructive we reduce the trap to two infinitesimally thin attractive δ potentials. δ functions have often been used to gain deeper insight with simple solutions [4,5,16,32–41]. By coupling the main system to a condensate outside the potential well we allow the particle exchange caused by the non-Hermitian potentials. Both the coupling mechanism and the environment will be constructed in a detailed fashion.

We use the Gross-Pitaevskii equation (GPE) to describe a BEC of particles with a short-ranged contact interaction. This equation describes a many-particle system in a mean-field approximation [42,43]. Due to the contact interaction of the atoms in the dilute gas the GPE exhibits a nonlinearity proportional to the modulus squared of the wave function. We note that the presence of $\mathcal{PT}$-symmetry in nonlinear systems is not trivial since the wave function appears in the Hamiltonian and thus also influences the symmetries. The important properties of $\mathcal{PT}$-symmetric systems, however, can still be observed when the eigenfunctions render the nonlinear term in the GPE $\mathcal{PT}$ symmetric [28]. In our case this means that the wave functions must have a symmetric modulus squared, which is fulfilled for real chemical potentials [44].

The basic outline of this article is as follows. We first summarize the properties of the non-Hermitian double-δ potential and its eigenstates in Sec. II. In Sec. III we introduce and discuss the coupling approach mentioned above. The results are then applied in Secs. IV and V to create different environments that can sustain an eigenstate of the double-δ potential. Finally simulations of the composite system of environment and stationary state are evaluated. A discussion of the results and their relation to physical units is added in Sec. VI.

*holger.cartarius@itp1.uni-stuttgart.de

II. NON-HERMITIAN DOUBLE-δ POTENTIAL

To describe the condensate we use the Gross-Pitaevskii equation in the dimensionless form introduced in [27]. Its time-dependent and time-independent versions read

$$i\frac{\partial}{\partial t}\psi = [-\Delta - g|\psi|^2 + V(x)]\psi, \tag{2a}$$

$$\mu\psi = [-\Delta - g|\psi|^2 + V(x)]\psi, \tag{2b}$$

respectively, where μ is the chemical potential. An attractive interaction is represented by a positive choice of the nonlinearity parameter g. When the system is confined to one dimension, this parameter can be adjusted by changing the trap frequencies confining the BEC [45]. We use a double-δ potential to represent the double well,

$$V(x) = (V + i\Gamma)\delta(x - a) + (V - i\Gamma)\delta(x + a). \tag{3}$$

This model has been used previously and proved to reproduce all important features of double-well potentials with finite width [27]. The system has three control parameters, i.e., the total distance between the two wells $2a$, and the real and imaginary parts of the potential, V and Γ, respectively. In this paper the values $a = 1.1$ and $V = -1.0$ are used, i.e., the unit of energy is chosen such that the real part of the prefactor of the δ functions in the potential is normalized to unity. Due to the non-Hermiticity parameter Γ the potential models a particle source at $x = a$ and a particle drain at $x = -a$. The nonlinearity g in the GPE (2) can be seen as a fourth parameter.

As found in [26] this system exhibits stationary states with real eigenvalues for nonzero g as long as the non-Hermiticity is not too strong. Like in the linear regime ($g = 0$), where analytic solutions are available, a ground state and an excited state exist. Both are $\mathcal{PT}$ symmetric. Figure 1 shows how the eigenvalues μ of these states depend on the parameter Γ when

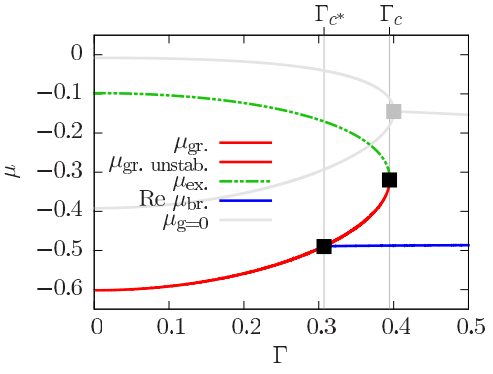

FIG. 1. (Color online) Eigenvalues μ of the double-δ potential in dependence of the non-Hermiticity parameter Γ. The spectrum is shown for $g = 1.0$ (nonlinear case, strong and colored lines) and $g = 0.0$ (linear case, light gray solid lines). Other parameters are fixed to $a = 1.1$ and $V = -1.0$. The spectrum consists in both cases of a ground state $\mu_{\rm gr}$ and an excited state $\mu_{\rm ex}$ which merge in an exceptional point at Γ_c. Above a critical value Γ_{c^*}, where $\Gamma_{c^*} < \Gamma_c$ for $g \neq 0$, two $\mathcal{PT}$-broken solutions with complex and complex-conjugate chemical potentials $\mu_{\rm br}$ appear, of which only the real part is shown in the figure. Ground-state solutions between both critical points Γ_c and Γ_{c^*} are unstable ($\mu_{\rm gr\ unstab}$). All values are given in the dimensionless units introduced in Ref. [27].

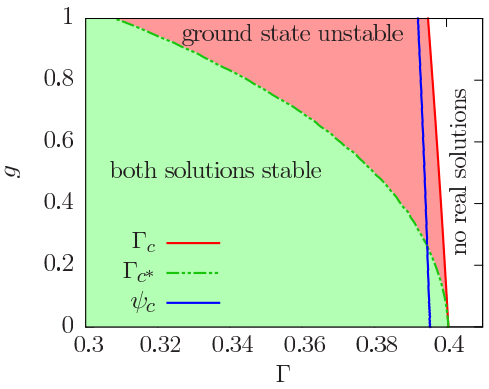

FIG. 2. (Color online) Parameter space of the double-δ potential for fixed $a = 1.1$ and $V = -1.0$. The dimensionless units introduced in Ref. [27] are used for all values. In the shaded areas stationary states with real eigenvalues exist. The lines separating the different areas show the location of the two critical points Γ_c and Γ_{c^*}. Between these critical points the ground-state solutions are unstable. The figure also shows where stationary states that satisfy relation (15) in Sec. V B can be found (ψ_c). Many of these solutions are in the unstable regime (upper shaded area).

all other system parameters are fixed. With increasing non-Hermiticity Γ the energy gap between those states becomes smaller. Eventually Γ reaches a critical value Γ_c at which the eigenvalues as well as the wave functions of both states coalesce. Further considerations show that this point fulfills all conditions of an exceptional point [46]. Beyond this branch point the branches with real μ vanish. In the linear regime it is also the point where the $\mathcal{PT}$-broken states appear. These states have eigenvalues $\mu_{\rm br}$ with a nonvanishing imaginary part. For nonzero g they branch off at another critical point $\Gamma_{c^*} < \Gamma_c$. This critical point is closely related to a stability change of the ground state, which can be shown using a linear stability analysis [47]. For values $\Gamma < \Gamma_{c^*}$ the ground state turns out to be dynamically stable with respect to small perturbations, above it is unstable. The stability of the excited state does not depend on Γ. Figure 2 shows the different stability regimes in parameter space together with the location of the critical points.

III. COUPLING APPROACH

Non-Hermitian potentials represent particle sources or drains. Because particles cannot just appear or vanish, such a potential can only be realized by an environment that exchanges particles with the system. We model such an environment using additional one-dimensional wave functions. In the following discussion we will assume that an overlap of the stationary state with its environment exists only in a δ-shaped trap, cf. Fig. 3. Thus, the interaction between the wave functions is confined to a single coupling or intersection point x_0. The sketch in Fig. 3 indicates one possible geometry with which this can be obtained. Two condensates with a confinement producing quasi-one-dimensional waves are arranged such that their extensions are orthogonal to each other and overlap in one point. In the equations we reduce everything to one dimension and use the same spatial coordinate for both

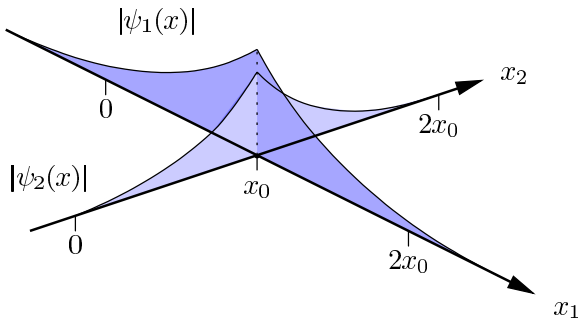

FIG. 3. (Color online) Sketch of the geometric alignment of two one-dimensional stationary states $\psi_1(x)$ and $\psi_2(x)$. Both states intersect at x_0 in their coordinate system and interact at this point.

wave functions to simplify the discussion. Since the waves only interact at a single point x_0 (or two separated points in the further discussion) the one-dimensional description can correctly reproduce the physical situation shown in Fig. 3.

In this section we discuss the form of the interaction and which requirements an environment must satisfy to replace the non-Hermitian part of a single-δ potential. The results are then used to model environments for the $\mathcal{PT}$-symmetric double-δ potential. Let $\psi_1(x)$ be a stationary solution of the GPE (2b) with the potential $V_{\text{eff},1}(x) = (V + i\Gamma)\delta(x - x_0)$ and the eigenvalue μ_1. We introduce another stationary state $\psi_2(x)$ acting as the environment. This state is assumed to be exposed to the potential $V_{\text{eff},2}(x) = (V + i\tilde{\Gamma})\delta(x - x_0)$ and to have the chemical potential μ_2. Note that $\tilde{\Gamma}$ is not known yet, it will be derived later. The parameters Γ and $\tilde{\Gamma}$ are supposed to describe the flux between both wave functions, i.e., an influx to one wave and an outflux from the other. We introduce a linear coupling between both wave functions at the intersection point. At the same time we remove all non-Hermitian contributions from the potential, which leads to the following system of equations:

$$\mu_1\psi_1 = [-\Delta - g|\psi_1|^2 + V\delta(x - x_0)]\psi_1 + \gamma\psi_2\delta(x - x_0), \tag{4a}$$

$$\mu_2\psi_2 = [-\Delta - g|\psi_2|^2 + V\delta(x - x_0)]\psi_2 + \gamma\psi_1\delta(x - x_0). \tag{4b}$$

The interaction strength is controlled by the coupling parameter γ. One can easily see that the following condition must be satisfied to reproduce $V_{\text{eff},1}(x)$ for $\psi_1(x)$:

$$i\Gamma = \gamma\frac{\psi_2(x_0,t)}{\psi_1(x_0,t)}. \tag{5}$$

From this we can derive several conditions that $\psi_2(x)$ has to fulfill. By demanding that γ is a real number we find a phase relation between both wave functions at the interaction point,

$$\arg\psi_2(x_0) - \arg\psi_1(x_0) = \pm\frac{\pi}{2}. \tag{6}$$

It is possible to choose γ complex, but this would needlessly complicate this relation and yield equivalent results. The real coupling parameter is used to parametrize the strength of the mechanism. All phase information is contained in the phase relations of the wave functions. Depending on the sign chosen in Eq. (6) we obtain a different sign for γ,

$$\gamma = \pm\Gamma\left|\frac{\psi_1(x_0)}{\psi_2(x_0)}\right|. \tag{7}$$

From now on we choose the phase between both wave functions at the interaction point such that γ is positive. This simplifies the discussion below. The implications of this choice will be discussed later when it actually yields consequences. Finally Eqs. (7) and (4b) can be used to calculate $\tilde{\Gamma}$ and the potential $V_{\text{eff},2}(x)$ for $\psi_2(x)$,

$$V_{\text{eff},2}(x) = \left(V - i\Gamma\left|\frac{\psi_1(x_0)}{\psi_2(x_0)}\right|^2\right)\delta(x - x_0). \tag{8}$$

The sign of the imaginary part originates from Eq. (6) and is always negative independent of the sign chosen in that phase relation. It should be emphasized that $V_{\text{eff},2}(x)$ depends on $\psi_1(x_0)$. This means that there is no universal environment because a change of $\psi_1(x)$ changes $V_{\text{eff},2}$ which eventually changes $\psi_2(x)$. Since both states are stationary, conditions (5) and (6) can only be satisfied for all times if the states possess the same chemical potential,

$$\mu_2 = \mu_1. \tag{9}$$

Despite the asymmetry in $V_{\text{eff},1/2}$ the total system (4) is closed and Hermitian. One can easily check that the particle or probability flux between both systems at the interaction point is opposite in sign and equal in strength. A stationary state can be coupled to several others, replacing an arbitrary number of non-Hermitian δ potentials. The wave functions that are used to create this environment will hereafter be called feeders. Using this method we can now construct an environment that can support a stationary state of the non-Hermitian double-δ potential. This can be done by either using two feeders, one for each well, or with only a single feeder. Both methods will be investigated.

IV. SEPARATE WAVE FUNCTIONS FOR EACH WELL

First we model an environment for a stationary solution of the double-δ potential $\psi_1(x)$ using one additional wave function for each δ peak. The incoming beam $\psi_2(x)$ transports particles from a distant reservoir to the well at $x = a$. Experimentally this could be realized with the use of Bragg beams, outcoupled from a condensate fraction trapped in a third well not part of the system investigated here [48]. Another beam $\psi_3(x)$ is used to remove particles at $x = -a$. The whole system is described by the following set of equations:

$$\mu\psi_1 = \{-\Delta - g|\psi_1|^2 + V[\delta(x - a) + \delta(x + a)]\}\psi_1 + \gamma\psi_2\delta(x - a) + \tilde{\gamma}\psi_3\delta(x + a), \tag{10a}$$

$$\mu\psi_2 = [-\Delta - g|\psi_2|^2 + V\delta(x - a)]\psi_2 + \gamma\psi_1\delta(x - a), \tag{10b}$$

$$\mu\psi_3 = [-\Delta - g|\psi_3|^2 + V\delta(x + a)]\psi_3 + \tilde{\gamma}\psi_1\delta(x + a). \tag{10c}$$

Since the beam is directed it is reasonable to assume that $\psi_3(x)$ quickly vanishes on one side of the interaction point, i.e., for $x \to -\infty$. We shall make the same assumption for the

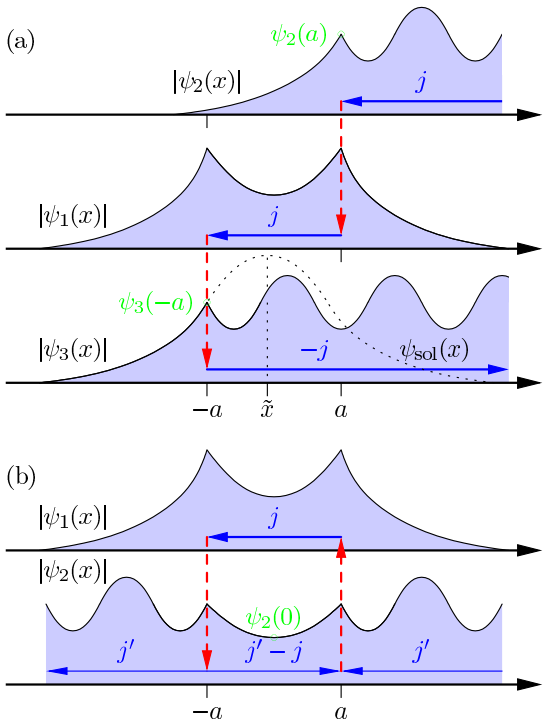

FIG. 4. (Color online) Both figures show an environment supporting a stationary state ψ_1 of the double-δ potential. Particle currents j are represented by solid blue arrows. Dashed red arrows represent a particle exchange between two wave functions. The free parameters for creating the environments are indicated as green dots. In (a) the environment consists of two feeders, particles are incoming via $\psi_2(x)$ and leaving via $\psi_3(x)$. In (b) the environment consists of only one wave function. The current it is carrying is partially redirected through $\psi_1(x)$. Figure (a) features a sketch of how $\psi_3(x)$ is constructed with use of the soliton solution (11) (black dotted line). Its maximum $\tilde{x}$ is positioned such that the correct function value at the coupling point is achieved.

incoming wave, which means that we expect the incoupling to be perfect. To be precise, the whole flux of the incoming beam is directed into $\psi_1(x)$. This will later simplify the stability optimization and render the discussion more instructive. In principle any imperfect incoupling can be compensated for by a larger amplitude of the incoming wave. It also means that all three wave functions carry the same particle current j. A sketch of the setup is depicted in Fig. 4(a).

The only stationary solution of the potential-free GPE with $g > 0$ at hand that satisfies $\lim_{x\to\pm\infty}\psi(x) = 0$ is the bright soliton solution

$$\psi_{\rm sol}(x) = \sqrt{\frac{2\kappa^2}{g}}\,\mathrm{sech}[\kappa(x-\tilde{x})], \quad \kappa^2 = -\mu. \tag{11}$$

Only this function can describe the feeders $\psi_{2/3}(x)$ on the side of the interaction point on which they vanish. We construct $\psi_{2/3}(x)$ by choosing the function value at the interaction points $\pm a$ [$+a$ for $\psi_2(x)$ and $-a$ for $\psi_3(x)$)]. Consequently this value must be chosen from the interval $(0,\sqrt{2\kappa^2/g}]$. This is done by shifting the maximum $\tilde{x}$ of the soliton (11) appropriately. Recall that the stationary GPE (2b) is a

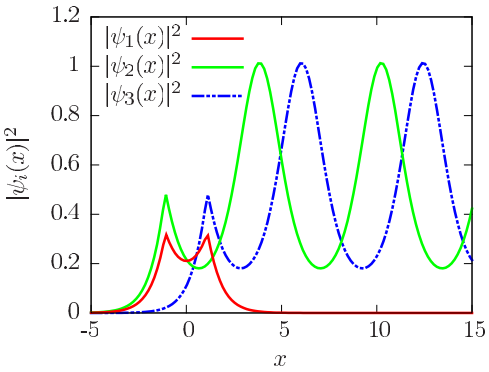

FIG. 5. (Color online) Squared moduli of a stationary ground state of the double-δ potential $\psi_1(x)$ and the two feeders $\psi_2(x)$ and $\psi_3(x)$. The numerical data were created with the parameters $a = 1.1$, $g = 1.0$, $\Gamma = 0.1$, and $\psi_{2/3}(\pm a) = 0.7$, which are given as all values in the figure in the dimensionless units introduced in Ref. [27].

second-order differential equation. This means that a function value $\psi_{2/3}(\pm a)$ and the value of the derivative $\psi'_{2/3}(\pm a)$ are enough to determine $\psi_{2/3}(x)$ completely. Since we require the form of the bright soliton solution, even one of these values is sufficient. The value of $\psi'_{2/3}(\pm a)$ can be derived from the value of $\psi_{2/3}(\pm a)$ as is explained in Appendix B. Thus, after choosing the function value the feeders can be integrated to the left. Integration to the right can be done after taking the potential $V_{\mathrm{eff},2/3}(x)$ into account. This potential features a δ peak at the interaction point, which causes a jump of the derivative. Figure 4(a) shows how the soliton solution is used to partially construct $\psi_3(x)$. The final construction step is to choose the global phase of $\psi_{2/3}(x)$ such that the phase relation (6) is fulfilled. In an experiment this phase could be changed by moving the double well along the beams $\psi_{2/3}(x)$.

A system constructed in this way can be seen in Fig. 5, where a stationary state of the double-δ potential (solid red line) and both feeders (dashed and dashed-double-dotted lines) are plotted. Here both feeders were created with the same function value at their interaction point. Note that the squared moduli of both feeders are almost the same, they are only translated in space. Apart from the translation the only difference between both waves is the direction of the current they carry. The reason for this symmetry originates from the construction of the feeders. On the right-hand side of both δ functions we require the soliton solution (11). The soliton wave ψ_3 has to possess the same function value at its coupling point $x = a$ as the wave ψ_2 at $x = -a$ to ensure that the in- and outfluxes are balanced. Due to the complex-conjugate action of the δ functions the feeders evolve on the right-hand side of their coupling points with the same moduli but different phases.

Each environment of this kind has the free parameters $\psi_{2/3}(\pm a)$ which can be picked such that certain properties of the feeders are optimized. The most important property is their stability or their tolerance with respect to perturbations. These feeders can be separated into two parts, one on each side of the δ potential. On the left side the wave function is described by the soliton solution while an unbound state of the potential-free GPE describes it on the other side. The soliton solution itself is stable, as observed in [49,50]; however, the

stability of the unbound solutions can only be determined in a numerical time evolution, which we performed.

In the numerical simulations the waves possess a finite lifetime after which they lose their stationary character due to numerical fluctuations in the simulation. Stable solutions are characterized by damping these tiny perturbations such that fluctuations are never observable. Unstable solutions are destroyed since the perturbations increase with time. For details about the simulation see Appendix A. We found that the environment states are in many cases sufficiently stable to provide the in- and outflux of the condensate fraction required for the implementation of imaginary potentials. However, appropriate feeders have to be selected carefully. The free parameters $\psi_{2/3}(\pm a)$ can be chosen in such a way that the highest possible lifetime is achieved. This in particular requires $\psi_2(a) = \psi_3(-a)$ or $\tilde{\gamma} = \gamma$ because then both feeders have an equivalent unbound part in terms of stability. With this optimization we found environments that were capable of sustaining $\psi_1(x)$ for roughly 10 reduced time units.

V. COUPLING TO ONE WAVE FUNCTION

A. Coupling to one unbound wave function

It is also possible to create environments that only consist of one wave function $\psi_2(x)$. This wave function then has two coupling points, one for each non-Hermitian δ potential it has to replace. For geometrical reasons alone, an experimental realization of such a system is certainly more challenging. We still perform this analysis because it is interesting from a theoretical point of view. Is it possible to create an environment consisting of only one wave function to replace a $\mathcal{PT}$-symmetric potential which must allow for spatially separated source and drain effects?

The system is described by two coupled equations, viz.,

$$\mu\psi_1 = \{-\Delta - g|\psi_1|^2 + V[\delta(x-a)+\delta(x+a)]\}\psi_1 + \gamma[\delta(x-a)+\delta(x+a)]\psi_2, \tag{12a}$$

$$\mu\psi_2 = \{-\Delta - g|\psi_2|^2 + V[\delta(x-a)+\delta(x+a)]\}\psi_2 + \gamma[(x-a)+\delta(x+a)]\psi_1. \tag{12b}$$

As at the end of Sec. IV we shall use only one value of γ for both interaction points. Together with the symmetry of $|\psi_1(x)|$ this imposes a condition on $\psi_2(x)$, viz.,

$$|\psi_2(-a)| = |\psi_2(a)|, \tag{13}$$

which in return renders $V_{\text{eff},2}(x)$ $\mathcal{PT}$ symmetric, see Eqs. (7) and (8). This means $\psi_2(x)$ has to be a stationary state of the $\mathcal{PT}$-symmetric double-δ potential. But these states are unbound, unlike those discussed in Sec. II. Figure 4(b) shows a sketch of an unbound feeder with two interaction points.

Before constructing the feeder we choose the state $\psi_1(x)$ for which we create the environment. Now that $\psi_2(x)$ has two interaction points, the phase relation (6) needs to be satisfied at both points, which is only possible if

$$\arg\psi_2(a) - \arg\psi_2(-a) = \arg\psi_1(a) - \arg\psi_1(-a) + \pi. \tag{14}$$

If two distinct values (or even one negative value) of γ were allowed, this relation would look different and lead to different environments. However, a discussion of all possible environments would exceed the scope of this work. Condition (13) can easily be satisfied by demanding that $|\psi_2(x)|$ has an extremal value at $x = 0$ because solutions of the GPE without potential are $\mathcal{PT}$ symmetric. We found that we can construct such an extremal value by choosing $\psi_2(0)$ real and $\psi_2'(0)$ purely imaginary. Both of these values were used as initial values for the numerical integration of $\psi_2(x)$. Fulfilling relation (14) is a more difficult task which we tackled by a numerical analysis using both initial values as variables. This analysis revealed that for any given $\psi_2(0)$ exactly one $\psi_2'(0)$ exists such that $\psi_2(x)$ satisfies this relation. Consequently, the choice of $\psi_2(0)$ already defines the whole function. The final construction step is to set the global phase of $\psi_2(x)$ in such a way that condition (6) is fulfilled.

Again there is one free parameter, $\psi_2(0)$, used in the creation of $\psi_2(x)$. This parameter was used to optimize the stability of the system. We were able to simulate systems with the excited $\mathcal{PT}$-symmetric stationary state for roughly 45 reduced time units. An example is shown in Fig. 6. The stationary $\mathcal{PT}$-symmetric state and its required feeder are plotted in Fig. 6(a). The temporal evolution of both wave functions can be found in Fig. 6(b), where density diagrams are drawn. A long and stable numerical evolution was possible because the unbound states that make up $\psi_2(x)$ could all be chosen to have a long lifetime, i.e., they can be propagated numerically stable. Without the optimization the system usually shows a numerical collapse as early as $t = 5$. The environments for the ground states are generally more unstable, resulting in lower numerical lifetimes ($t \approx 10$) for these states until large fluctuations appear and destroy the wave functions. To improve these lifetimes we suggest studying such systems with a different choice of a and V or by the use of two different signs of γ for each interaction point.

B. Coupling to one bound wave function

So far we assumed that all environments made from one wave function are unbound. In this section we show that it is even possible to find bound feeders. We found these solutions in an extensive numerical study, but some properties can already be understood by a few simple considerations. We know that both wave functions are stationary states of the double-δ potential. Also both $\psi_1(x)$ and $\psi_2(x)$ must have the same energy eigenvalue. Since the spectrum of the double-δ potential is nondegenerate (see Fig. 1) $\psi_2(x)$ can only be equal to $\psi_1(x)$ or $\psi_1(-x)$. Only the latter approach is consistent with relation (14). With this ansatz the phase relation turns into a condition for $\psi_1(x)$, viz.,

$$\arg\psi_1(a) - \arg\psi_1(-a) = \pi/2. \tag{15}$$

Only wave functions $\psi_1(x)$ that fulfill this condition can be coupled to the bound environment. The position of these states in parameter space is labeled ψ_c in Fig. 2. They are located very close to the critical point Γ_c and their non-Hermiticity parameter is very large, with a value of $\Gamma \approx 0.39$. All of these states belong to the ground-state branch, which is why many of them are unstable (cf. Fig. 2). This situation may change if the parameters a and V are chosen differently. We note that the time evolution of these systems could not

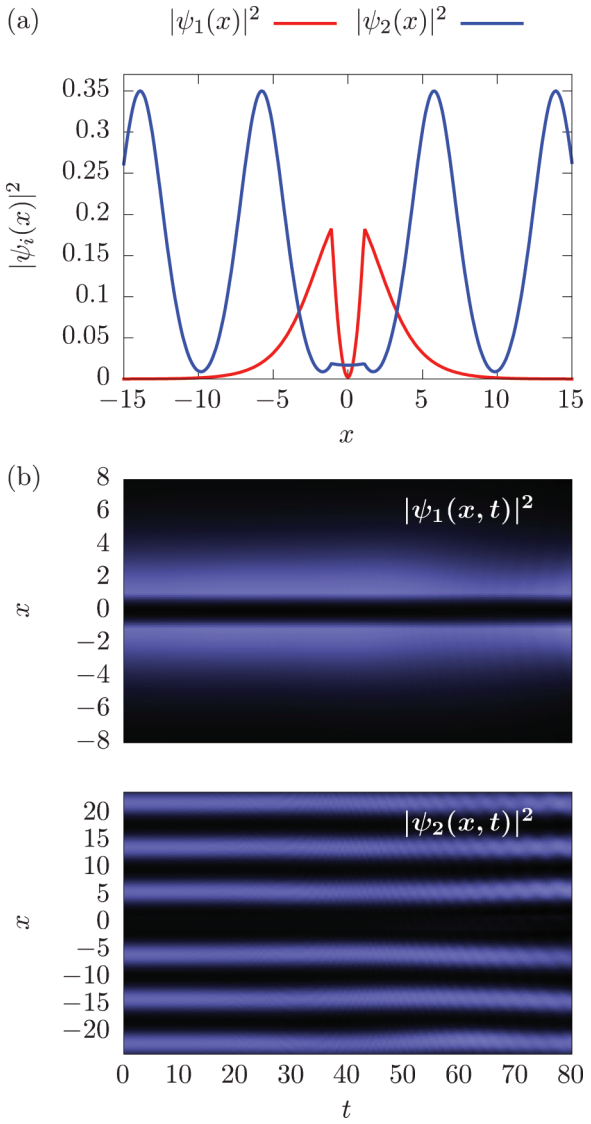

FIG. 6. (Color online) (a) Modulus squared of a stationary state of the double δ potential $\psi_1(x)$ and its feeder $\psi_2(x)$. (b) Simulated time evolution of both states. The system parameters in the dimensionless units from Ref. [27] used in the figure are $a = 1.1$, $V = -1.0$, $\Gamma = 0.1$, and $g = 1.0$. Numerical perturbations cause both states to develop fluctuations, thus destroying the dynamics. They lose the stationary property at $t \approx 45$. Bright colors represent high probability amplitudes; compare with (a) for absolute values.

be simulated correctly because of the large non-Hermiticity parameter. Large values of Γ caused errors in our simulations originating from the singular character of the δ functions. This is explained in more detail in Appendix A.

VI. DISCUSSION AND OUTLOOK

We successfully used a linear coupling scheme to replace non-Hermitian δ potentials for BECs in a double-well setup. This coupling allowed a particle exchange with an environment consisting of one or two additional wave functions. Several methods to construct such wave functions for stationary solutions of the double-δ potential were discussed. The individual results were then tested in numerical simulations that maintained the correct behavior for a certain time span. After this time numerical perturbations caused unwanted dynamics, destroying the stationary character of the system. The time this takes depends on the environment and the way it is constructed.

For comparison with a realistic setup we present the time in SI units for a dilute BEC of 5000 ^{87}Rb atoms and a distance of $2a = 2.2\ \mu$m between both potential wells. Then the longest stable simulation was done with an unbound environment consisting of one wave function and it lasted for an equivalent of 123 ms. Other systems with two additional wave functions could be simulated for up to 27 ms before the stationary character of the system was lost. The simulations reveal that the mechanism works well for a limited time.

We were able to simulate single unbound states for a longer time period than the compound systems and found that the singular character of the δ potentials shortens this time considerably (cf. Appendix A). A remedy could be a consideration of a system in which potentials with finite width are used. This approach will be the next step in extending the model. A more detailed stability analysis of the unbound solutions of the potential-free GPE could also yield results that could be used to improve this model further.

The results presented here are clearly only a first step toward the possibility of realizing a $\mathcal{PT}$-symmetric potential with a coupling of a BEC to condensate fractions outside the double well. The approach provides an alternative to that suggested in Refs. [51,52] where the $\mathcal{PT}$-symmetric double well was considered to be embedded in a four-well structure. The results presented here are very encouraging since they demonstrate the applicability of the approach. More realistic setups in three dimensions with a specific description of the reservoir providing the environment are necessary to gain more insight into possible experimental realizations.

APPENDIX A: SIMULATION

The time evolution of all systems was simulated using the split operator method. In this method the time evolution operator $e^{-iH\Delta t}$ is approximated by the Baker-Campbell-Hausdorff formula

$$|\psi(t+\Delta t)\rangle = e^{-iH\Delta t}|\psi(t)\rangle = e^{-i[p^2+V(x)]\Delta t}|\psi(t)\rangle$$
$$= e^{-ip^2\frac{\Delta t}{2}}\, e^{-iV(x)\Delta t}\, e^{-ip^2\frac{\Delta t}{2}}\, e^{O(\Delta t^3)}|\psi(t)\rangle.$$

This approximation is suitable for a numerical evaluation because it is a consecutive execution of operators that operate only in position *or* momentum space. A switch between both spaces via a fast-Fourier transformation reduces the application of the operators to simple multiplications.

In our simulations the wave function was discretized into 16 384 or 32 786 bins. The time step Δt was chosen between 10^{-6} and 10^{-4} depending on the problem. We used a large number of bins to obtain a high resolution in position space in the simulations containing δ functions. A δ potential $a\delta(x - x_0)$ was implemented by setting the value of the potential at the bin closest to x_0 to $a/\Delta x$, where Δx is the resolution in position space. The nonlinear interaction term of the GPE (2) was implemented as a time-dependent potential.

We tested this simulation by evolving stationary states of the double-δ potential. These tests revealed that the method works well if the non-Hermiticity parameter Γ is small. Large values quickly caused small numerical perturbations to become too large, yielding wrong simulation results. After extensive numerical tests we can relate these effects completely to the singular character of the δ potentials. Combined with non-Hermitian terms small errors then lead to an irreversible change of the norm instead of a reversible redistribution of the energy. While δ potentials are easy to handle in an analytical approach they are hard to implement in a discrete numerical computation. Because of these purely numerical errors we restrict our simulation to potentials with small Γ, usually $\Gamma = 0.1$.

We also used the simulation to investigate the stability behavior of unbound solutions of the potential-free GPE (2b). In these simulations the wave functions eventually lose their stationary character indicating that they are unstable. The time it took for this to happen depended on the individual state and could be as small as 5 reduced time units. For some states it was independent of the simulation accuracy used. We classified these states as unstable. For other states this time increased when Δt was decreased or the number of bins was increased. These states were classified as potentially stable and could be simulated for up to 70 reduced time units.

APPENDIX B: SOLITON SOLUTION

In this section we derive an expression of the derivative of the soliton solution (11).

$$\frac{d}{dx}\psi_{\mathrm{sol}}(x) = -\sqrt{\frac{2\kappa^2}{g}}\,\mathrm{sech}[\kappa(x-x_0)]\tanh[\kappa(x-x_0)]$$
$$= -\kappa\,\psi_{\mathrm{sol}}(x)\tanh\left[\mathrm{arcsech}\left(\sqrt{\frac{g}{2\kappa^2}}\,\psi_{\mathrm{sol}}(x)\right)\right].$$

With the relation

$$\tanh \mathrm{arcsech} x = \pm\sqrt{1-x^2}, \tag{B1}$$

we gain an expression for ψ'_{sol} depending only on the function value and κ,

$$\frac{d}{dx}\psi_{\mathrm{sol}} = \kappa\,\psi_{\mathrm{sol}}\sqrt{1-\frac{g\psi_{\mathrm{sol}}^2}{2\kappa^2}}. \tag{B2}$$

This formula is used in the construction of the feeders in Sec. IV. It enables us to calculate the derivative of the wave function with the function value which acts as a free parameter in the construction of the feeders. Both values can then be used for the numerical integration of the wave function. Note that there are two solutions because of the square root. We only used the positive solution resulting in feeders as depicted in Fig. 4(a).

[1] N. Moiseyev, *Non-Hermitian Quantum Mechanics* (Cambridge University, Cambridge, England, 2011).
[2] C. M. Bender and S. Boettcher, Phys. Rev. Lett. **80**, 5243 (1998).
[3] H. F. Jones and E. S. Moreira, Jr., J. Phys. A **43**, 055307 (2010).
[4] V. Jakubský and M. Znojil, Czech. J. Phys. **55**, 1113 (2005).
[5] H. Mehri-Dehnavi, A. Mostafazadeh, and A. Batal, J. Phys. A **43**, 145301 (2010).
[6] C. M. Bender, S. Boettcher, and P. N. Meisinger, J. Math. Phys. **40**, 2201 (1999).
[7] G. Lévai and M. Znojil, J. Phys. A **35**, 8793 (2002).
[8] C. M. Bender, V. Branchina, and E. Messina, Phys. Rev. D **85**, 085001 (2012).
[9] P. D. Mannheim, Fortschr. Phys. **61**, 140 (2013).
[10] C. M. Bender, H. F. Jones, and R. J. Rivers, Phys. Lett. B **625**, 333 (2005).
[11] S. Bittner, B. Dietz, U. Günther, H. L. Harney, M. Miski-Oglu, A. Richter, and F. Schäfer, Phys. Rev. Lett. **108**, 024101 (2012).
[12] J. Schindler, A. Li, M. C. Zheng, F. M. Ellis, and T. Kottos, Phys. Rev. A **84**, 040101 (2011).
[13] J. Schindler, Z. Lin, J. M. Lee, H. Ramezani, F. M. Ellis, and T. Kottos, J. Phys. A **45**, 444029 (2012).
[14] K. G. Makris, R. El-Ganainy, D. N. Christodoulides, and Z. H. Musslimani, Int. J. Theor. Phys. **50**, 1019 (2011).
[15] K. G. Makris, R. El-Ganainy, D. N. Christodoulides, and Z. H. Musslimani, Phys. Rev. Lett. **100**, 103904 (2008).
[16] A. Mostafazadeh and H. Mehri-Dehnavi, J. Phys. A **42**, 125303 (2009).
[17] A. Mostafazadeh, Phys. Rev. A **87**, 063838 (2013).
[18] A. Mostafazadeh, Phys. Rev. Lett. **110**, 260402 (2013).
[19] E. M. Graefe, H. J. Korsch, and A. E. Niederle, Phys. Rev. Lett. **101**, 150408 (2008).
[20] E. M. Graefe, U. Günther, H. J. Korsch, and A. E. Niederle, J. Phys. A **41**, 255206 (2008).
[21] E. M. Graefe, H. J. Korsch, and A. E. Niederle, Phys. Rev. A **82**, 013629 (2010).
[22] Z. H. Musslimani, K. G. Makris, R. El-Ganainy, and D. N. Christodoulides, J. Phys. A **41**, 244019 (2008).
[23] A. Guo, G. J. Salamo, D. Duchesne, R. Morandotti, M. Volatier-Ravat, V. Aimez, G. A. Siviloglou, and D. N. Christodoulides, Phys. Rev. Lett. **103**, 093902 (2009).
[24] C. E. Rüter, K. G. Makris, and E.-G. Ramy, Nat. Phys. **6**, 192 (2010).
[25] S. Klaiman, U. Günther, and N. Moiseyev, Phys. Rev. Lett. **101**, 080402 (2008).
[26] H. Cartarius, D. Dast, D. Haag, G. Wunner, R. Eichler, and J. Main, Acta Polytech. **53**, 259 (2013).
[27] H. Cartarius and G. Wunner, Phys. Rev. A **86**, 013612 (2012).
[28] H. Cartarius, D. Haag, D. Dast, and G. Wunner, J. Phys. A **45**, 444008 (2012).
[29] D. Dast, D. Haag, H. Cartarius, G. Wunner, R. Eichler, and J. Main, Fortschr. Phys. **61**, 124 (2013).
[30] D. Haag, D. Dast, A. Löhle, H. Cartarius, J. Main, and G. Wunner, Phys. Rev. A **89**, 023601 (2014).
[31] R. Fortanier, D. Dast, D. Haag, H. Cartarius, J. Main, G. Wunner, and R. Gutöhrlein, Phys. Rev. A **89**, 063608 (2014).
[32] A. Mostafazadeh, J. Phys. A **39**, 13495 (2006).
[33] H. F. Jones, Phys. Rev. D **78**, 065032 (2008).
[34] T. Mayteevarunyoo, B. A. Malomed, and G. Dong, Phys. Rev. A **78**, 053601 (2008).

[35] K. Rapedius and H. J. Korsch, J. Phys. B **42**, 044005 (2009).
[36] D. Witthaut, K. Rapedius, and H. J. Korsch, J. Nonlinear Math. Phys. **16**, 207 (2008).
[37] S. Fassari and F. Rinaldi, Rep. Math. Phys. **69**, 353 (2012).
[38] E. Demiralp, J. Phys. A **38**, 4783 (2005).
[39] H. Jones, Phys. Lett. A **262**, 242 (1999).
[40] Z. Ahmed, Phys. Lett. A **286**, 231 (2001).
[41] H. Uncu, D. Tarhan, E. Demiralp, and Ö. E. Müstecaplioglu, Laser Phys. **18**, 331 (2008).
[42] E. P. Gross, Il Nuovo Cimento **20**, 454 (1961).
[43] L. P. Pitaevskii, Sov. Phys. JETP **13**, 451 (1961).
[44] D. Dast, D. Haag, H. Cartarius, J. Main, and G. Wunner, J. Phys. A **46**, 375301 (2013).
[45] T. Paul, M. Hartung, K. Richter, and P. Schlagheck, Phys. Rev. A **76**, 063605 (2007).
[46] W. D. Heiss, H. Cartarius, G. Wunner, and J. Main, J. Phys. A **46**, 275307 (2013).
[47] A. Löhle, H. Cartarius, D. Haag, D. Dast, J. Main, and G. Wunner, Acta Polytech. **54**, 133 (2014).
[48] Y. Shin, G. B. Jo, M. Saba, T. A. Pasquini, W. Ketterle, and D. E. Pritchard, Phys. Rev. Lett. **95**, 170402 (2005).
[49] K. E. Strecker, G. B. Partridge, A. G. Truscott, and R. G. Hulet, Nature **417**, 150 (2002).
[50] L. Khaykovich, F. Schreck, G. Ferrari, T. Bourdel, J. Cubizolles, L. D. Carr, Y. Castin, and C. Salomon, Science **296**, 1290 (2002).
[51] M. Kreibich, J. Main, H. Cartarius, and G. Wunner, Phys. Rev. A **87**, 051601(R) (2013).
[52] M. Kreibich, J. Main, H. Cartarius, and G. Wunner, Phys. Rev. A **90**, 033630 (2014).